

# **Transmission Grating Measurements of Undulator $K$**

**R. M. Bionta, L. L. Ott**

**May 15, 2006.**

## **Disclaimer**

This document was prepared as an account of work sponsored by an agency of the United States Government. Neither the United States Government nor the University of California nor any of their employees, makes any warranty, express or implied, or assumes any legal liability or responsibility for the accuracy, completeness, or usefulness of any information, apparatus, product, or process disclosed, or represents that its use would not infringe privately owned rights. Reference herein to any specific commercial product, process, or service by trade name, trademark, manufacturer, or otherwise, does not necessarily constitute or imply its endorsement, recommendation, or favoring by the United States Government or the University of California. The views and opinions of authors expressed herein do not necessarily state or reflect those of the United States Government or the University of California, and shall not be used for advertising or product endorsement purposes.

## **Auspices Statements**

This work was performed under the auspices of the U.S. Department of Energy by University of California, Lawrence Livermore National Laboratory under Contract W-7405-Eng-48. Work supported in part by the DOE Contract DE-AC02-76SF00515. This work was performed in support of the LCLS project at SLAC.

# Transmission Grating Measurements of Undulator $K$

R. M. Bionta, L. L. Ott

Lawrence Livermore National Laboratory

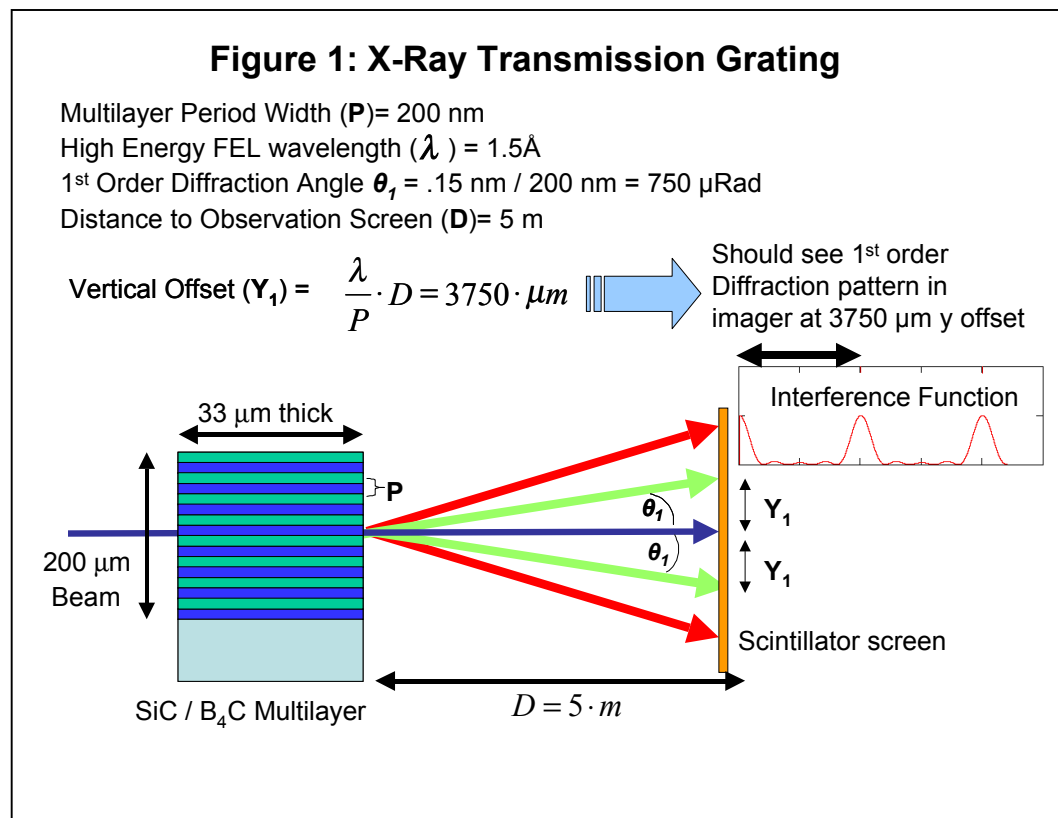
May 15, 2006

## Introduction

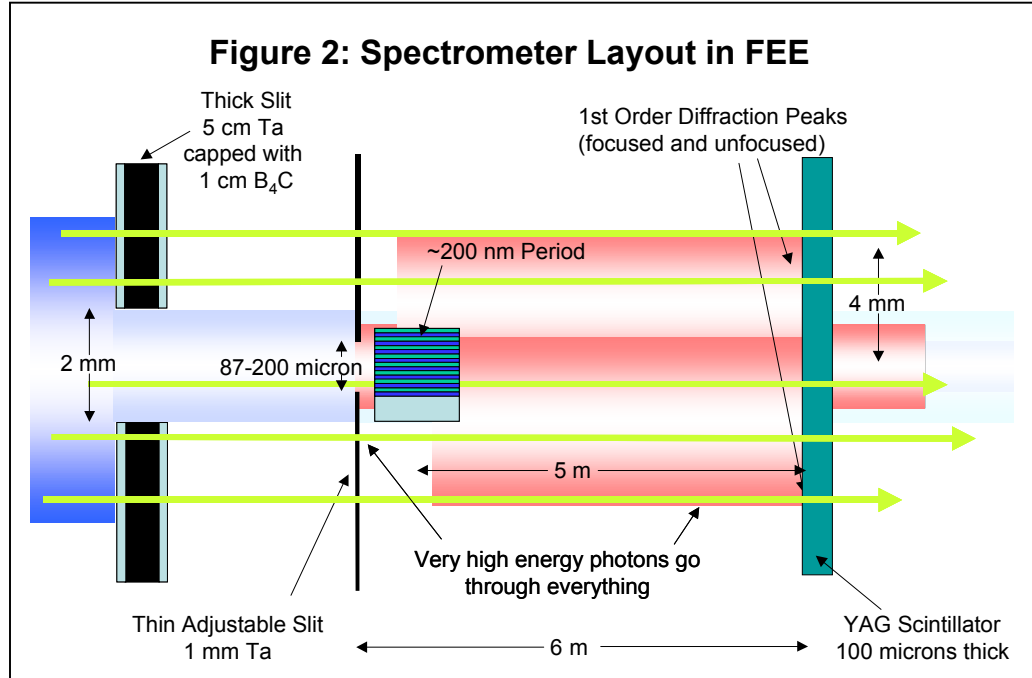
This study was undertaken to understand the practicalities of determine  $K$  differences in the undulator modules by measuring single-shot x-ray spectra of the spontaneous radiation with a transmissive grating spectrometer under development to measure FEL spectra. Since the quality of the FEL is dependent on a uniform  $K$  value in all the undulator modules, being able to measure the relative undulator  $K$  values is important. Preliminary results were presented in a presentation, "Use of FEL Off-Axis Zone Plate Spectrometer to Measure Relative  $K$  by the Pinhole/Centroid Method", at the "LCLS Beam-Based Undulator  $K$  Measurements Workshop" on November 14, 2005 (UCRL-PRES-217281). This study applies equally well to reflective gratings of the appropriate period and inclinations.

## FEL Spectrometer

The 8.26 keV FEL Spectrometer uses an x-ray transmission grating to disperse the x-ray beam into its spectral components as shown in Figure 1. The grating is made of alternating layers of SiC and B<sub>4</sub>C which are two of the materials expected to



survive full exposure to the saturated 8.26 keV FEL. The grating is manufactured by sputtering alternating layers of SiC and B<sub>4</sub>C and then slicing the multilayer perpendicular to the layers to a thickness of 33μm (along the beam direction.). The 33μm thickness was chosen so that the x-rays emerging from the SiC layers are π radians out of phase with respect to the x-rays emerging from the B<sub>4</sub>C layers. The interference caused by this phase difference causes the x-rays to be deflected in a wavelength dependent manner. The period of the grating varies slightly across its aperture according to the zone plate formula  $r_n = r_1 \cdot \sqrt{n}$ ,  $r_1 = \sqrt{\lambda \cdot f}$ , evaluated far off axis ( $n$  very large). This causes the x-rays to come to a sharper focus at the



observation screen. The section of the zone plate exposed to the beam has an aperture of 200 μm and an average period of approximately 200nm, the width of one layer of SiC and one layer of B<sub>4</sub>C. This gives a first order deflection for 8.261 keV radiation of 750 micro radians. The focal length,  $f$ , of the zone plate pattern was chosen to focus light from the center of the undulator onto an image plane 5 meters downstream of the grating. Thus light from the 8.261 keV fundamental will be deflected 3750 mm from the central ray at the image plane.

The FEL spectrometer containing the zone plate / grating was intended to be placed in the near hall but for K measurements must be placed in the white beam area of the Front End Enclosure (FEE) in order to have access to the raw spontaneous radiation from single undulator segments. The layout in the FEE used for K measurements with the transmission grating is shown in Figure 2. The grating sits in the diagnostics tank just downstream of a thin adjustable slit (Ta 1 mm thick) which is used to adjust the solid angle acceptance of 8 keV radiation striking the grating. Further upstream, the pair of thick slits blocks background high-energy spontaneous radiation from striking the detector in the region of the diffracted signal. Photons diffracted by the grating are imaged with a scintillation based

imager placed 5 meters downstream of the grating. The scintillator is a 100 micron thick YAG crystal imaged by a CCD camera with an assumed spatial resolution on the scintillator of 10 microns.

## Simulation

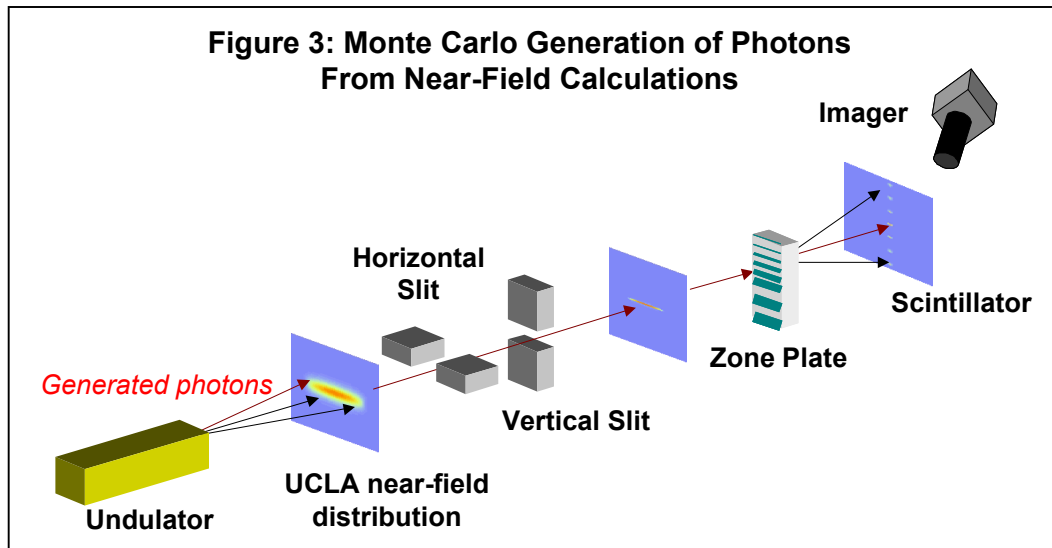
**Table 1: UCLA high resolution data sets**

Segment	K Value	$\Delta K/K$	DataSet
1	3.50350	Detuned by $10^{-3}$	FirstDet-3
1	3.50035	Detuned by $10^{-4}$	FirstDet-4
1	3.50000	Nominal	FirstNom
15	3.50350	Detuned by $10^{-3}$	MidDet-3
15	3.50035	Detuned by $10^{-4}$	MidDet-4
15	3.50000	Nominal	MidNom
33	3.50350	Detuned by $10^{-3}$	LastDet-3
33	3.50035	Detuned by $10^{-4}$	LastDet-4
33	3.50000	Nominal	LastNom

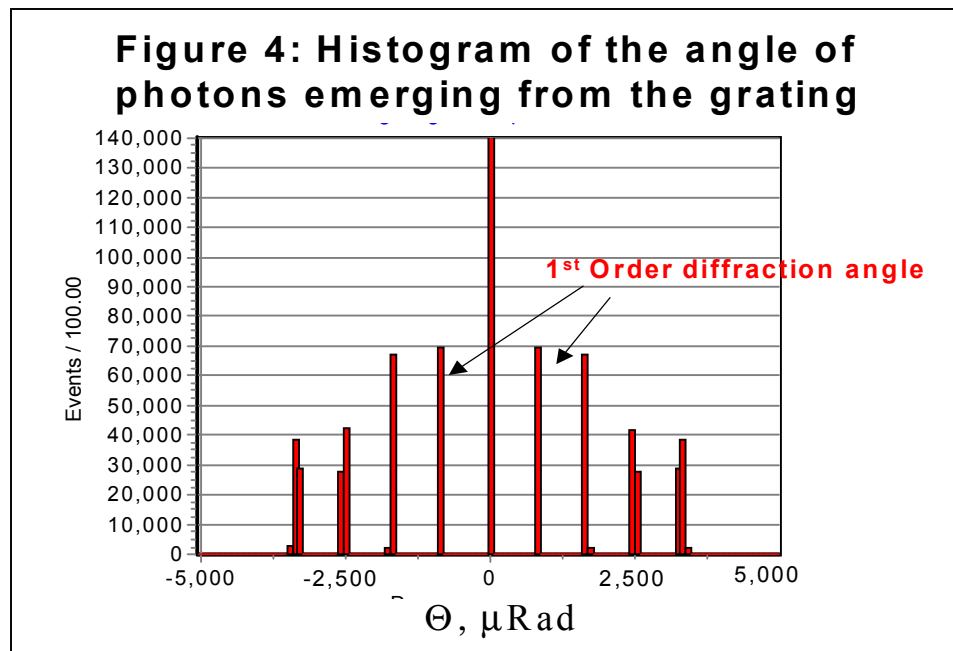
We simulated the spectrometer response to spontaneous radiation from single undulator segments with varying K values. First, Sven Reiche at UCLA calculated the single undulator spontaneous radiation spectral flux densities numerically at a linac energy of 13.64 GeV and a distance of 244 meters from the position of the beginning of the first undulator segment. Sven performed two kinds of calculations, table 1, one had an energy resolution of 1 eV and covered a small (2x2mm) grid transverse to the beam axis and the other set had a courser energy resolution of 400 eV and covered a larger, 120x40mm transverse spatial grid. The high resolution datasets cover the photon energy range from 0 to 30 keV. The courser resolution datasets cover an energy range from 1 to 24.7 MeV and are used to estimate the effects of high energy background radiation in the detector.

For the high resolution datasets, three undulator segments were modeled with three K settings each as summarized in table 1. The lower resolution background datasets were calculated for just the first and last undulator segments at the nominal K value.

Sven's data sets were fed into our Monte Carlo (MC) code that tracks individual photons from the undulator through the x-ray beam line vacuum pipe and optic elements. The MC simulates the photoelectric effect, Compton scattering, and reflection and refraction at the boundary between two materials. Separate MC runs model individual components or sub-assemblies. The MC models can be chained together by using the output from one MC as input to the next MC to build complicated beam line simulations to study various configurations.



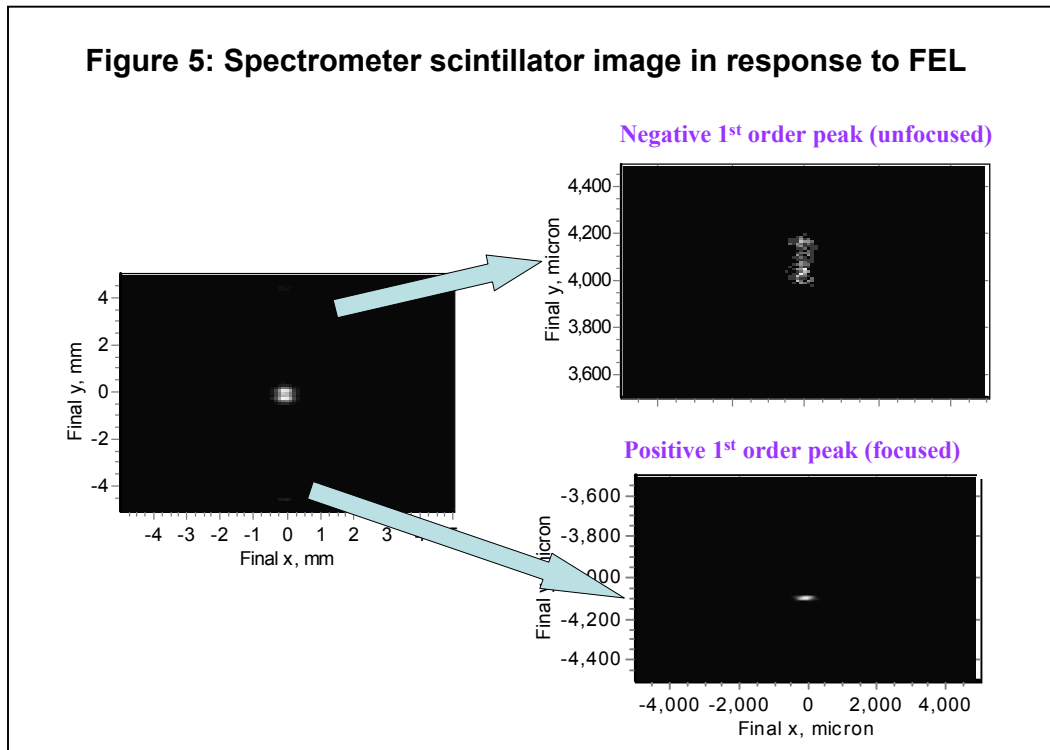
The MC generates simulated photons whose energy and angular distributions follow Sven's detailed spectral flux calculations. The generated photons are started inside the appropriate undulator segment (the first, middle or last segment) then tracked through the undulator vacuum chamber, the horizontal and vertical thick slits, the spectrometer, then through the scintillator plate (see figure 3.). The spectrometer MC model includes a horizontal and a vertical thin adjustable slit, the transmission zone plate and an yttrium-aluminium-garnet (YAG) scintillator plate. The thin adjustable slit is used to keep the total solid angle intercepted by the grating the same regardless of which undulator segment is generating the photons.



The diffraction grating is modeled as a stack of SiC and B<sub>4</sub>C layers. Photons that exit the stack are randomly diffracted into positive or negative diffraction orders with relative proportions taken from a pre-determined list of values. For these runs

the diffraction efficiency was assumed to be a uniform and equal 10% into each order from the  $-4^{\text{th}}$  to the  $+4^{\text{th}}$  including the  $0^{\text{th}}$  order. The photon deflection angle is calculated from the generated order and a small aperture-dependent random jitter is added to this angle to account for the diffraction limit of the zone plate. Figure 4 shows the resulting diffraction angle of photons exiting the grating for a typical MC simulation. The first order diffraction angle is close to  $750 \mu\text{Radian}$ .

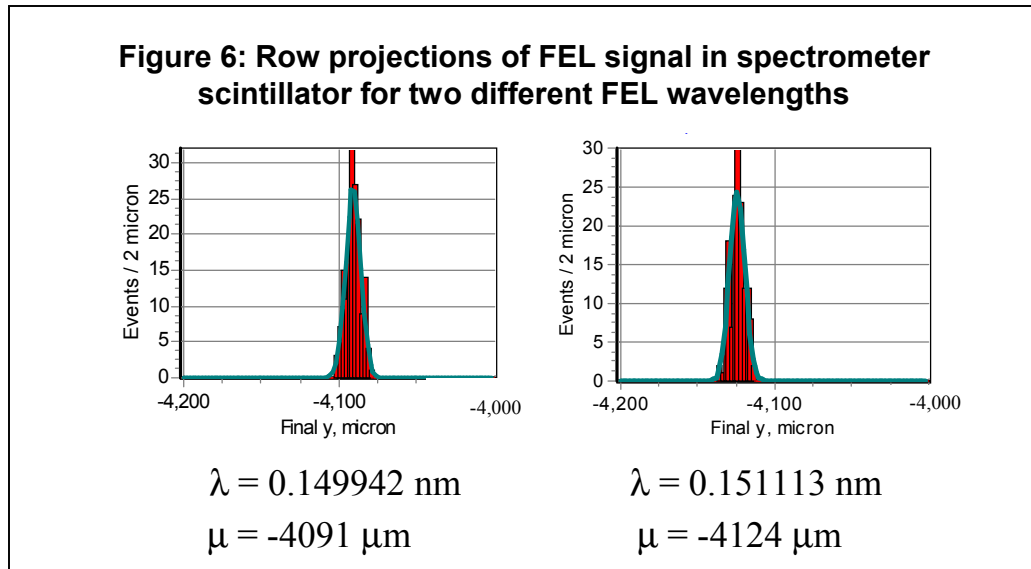
The photons are further tracked through the scintillator plate and beyond to the end of the simulation. The result of each Monte Carlo run is a histogram of the number of photons that stopped in the scintillator vs. position in the Region Of Interest (ROI) centered on the expected position of the diffracted 8.261 keV photons. The ROI is from  $-4,250 \mu\text{m}$  to  $-4,050 \mu\text{m}$  in the vertical direction and  $\pm 1 \text{ mm}$  in the horizontal direction. The  $200 \mu\text{m}$  length in the vertical direction is divided into 10  $\mu\text{m}$  bins to simulate the 10 micron detector resolution. The histogram is a simulation of the measured photon spatial distribution after diffraction by the grating and since the grating produces a correlation between photon energy and vertical position, the histogram simulates the photon energy spectrum as would be measured by performing a row projection of the data from a single shot camera image. By fitting the histogram to a Gaussian shape, the centroid position for the peak number of photons can be found with high precision. The object of this study is to determine whether or not this centroid position can be measured accurately enough to determine the relative K difference in individual undulator modules.



## Grating Performance with the FEL Beam

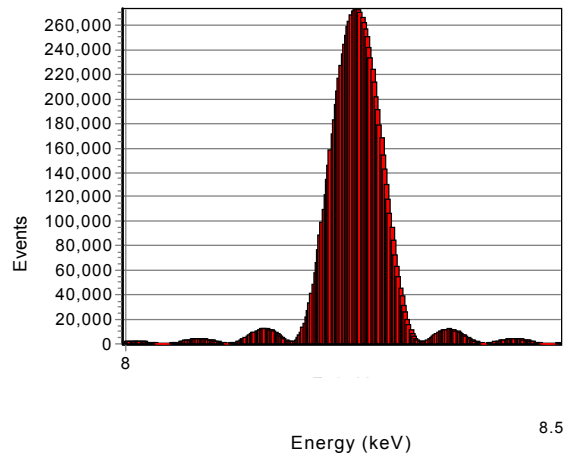
To illustrate the grating performance in a simple way we simulated its response to the 8.26 keV FEL, with no accompanying spontaneous radiation. Figure 5 shows the spatial distribution of the energy deposited in the scintillator by the photons traveling downstream of the grating. The image on the left covers a wide field-of-view (10 mm x 10 mm) containing the undiffracted beam in the center as well as the (very faint) positive and negative first order diffracted peaks above and below. The images on the right show the ROI around the positive (lower) and negative (upper) first order peaks. The focusing of the positive (lower image) and defocusing of the negative (upper image) orders is apparent.

Quantitative analysis on the focused imaged is done by first projecting the image along its rows to produce a histogram, figure 6, then fitting the histogram to a Gaussian shape to find the centroid and width. The figure shows the results for two different FEL energies differing by  $\Delta\lambda/\lambda = 8 \times 10^{-3}$ . The fitted sigma / mean is  $1.2 \times 10^{-3}$  consistent with the inverse of the number of zones intercepted by the FEL footprint. From the positions of the fitted centroids we obtain the spatial/energy conversion constant of 1.95 eV/micron.



## Grating Performance with the First Undulator Segment

**Figure 7: Simulated energy distribution of photons exiting the first undulator module at nominal  $K$  (from dataset FirstNom)**



The Off-Axis Spectrometer Monte Carlo model was used to generate  $10^7$  photons from the high-resolution near-field dataset, *FirstNom*, representing the first undulator module with a nominal  $K$  value. The figures in this section show the resulting scatterplots, histograms and fit values.

**Figure 8: Spectrometer scintillator response to spontaneous radiation from the first undulator segment at nominal  $K$**

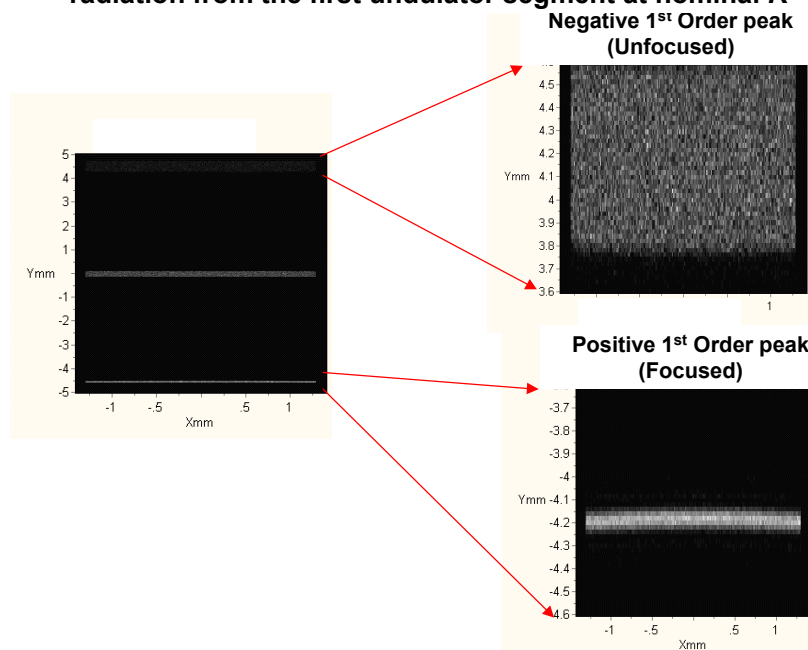
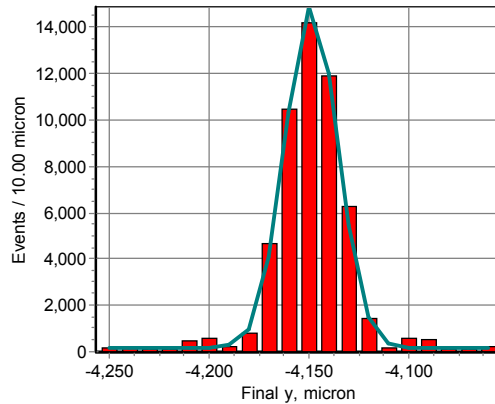




Figure 7 shows the MC generated distribution of photon energies for the first undulator segment at nominal  $K$  between 8.0 and 8.5 keV. This distribution contains all photons generated by the first undulator segment into the solid angle defined by a 2 x 2 mm square 114 meters beyond the position of the end of the last undulator segment. Since the sample is restricted to forward angles the distribution is very close to the  $\sin(x)/x$  shape. Its peak (for photons in the forward direction) is expected to shift in response to a change in  $K$  by  $\frac{\Delta E}{E_1} = 2 \cdot \frac{K^2}{2 + K^2} \cdot \frac{\Delta K}{K} \approx 1.7 \cdot \frac{\Delta K}{K}$ .

Figure 8 shows the spatial distribution of the photons that interacted in the scintillator. The image on the left is of a wide field of view centered on the undeflected beam and extending vertically to cover both the positive and negative first order peaks. The horizontal band in the middle consists of photons that passed through the grating without being absorbed and diffracted into 0<sup>th</sup> order. The size and shape of the 0<sup>th</sup> order band is determined by the size and shape of the thin slit aperture which was set to 200 microns horizontally by 200 microns vertically. The images on the right show expanded views of the regions of the positive and negative 1<sup>st</sup> order peaks. The unfocused negative 1<sup>st</sup> order, top right, is spread over more than a mm in the vertical direction. The focused positive first order, bottom right, shows a narrow band that is slightly curved in an upside-down U shape indicating higher photon energies (harder to bend) in the center, and lower photon energies (easier to bend) at larger  $x$ , away from the beam center. This is to be expected from the spontaneous radiation where the highest photon energies are found along the axis.

**Figure 9: Row projection of scintillator response across positive 1<sup>st</sup> order peak from the first undulator segment at nominal  $K$**



Fitted Centroid:  
-4148.70 ± 0.06 μm

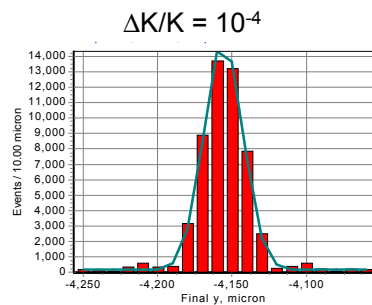
53,192 photons in Monte Carlo Simulation  
Scaled to Full Pulse: 135,799 ± 588 photons

Figure 9 shows the row projection across the positive 1st order peak. The data have been binned in 10 micron bins to simulate a detector resolution of 10 microns. The  $\sin(x)/x$  shape of the energy distribution is apparent in the row projection. The solid line is the result of a Gaussian fit to the data. The centroid of the Gaussian was determined by the fit to be at  $-4148.70 \pm 0.06 \mu\text{m}$ .

The number of simulated photons that appear in this plot is 53192. The actual number of photons expected from a full 0.79 nC LCLS pulse is determined by scaling this number by the ratio of the number of photons in the 2 mm x 2 mm area as calculated by the near-field calculation to the number of photons generated in this area by the MC. The number of MC generated photons was  $10^7$ , while the near-field calculated number of photons of the same energy range in the 2 mm x 2 mm area is  $2.55 \times 10^7$ . Thus the number of photons in this simulation must be multiplied by 2.5 to obtain the number of photons expected with a 0.79 nC pulse. So the actual number of photons expected in a 0.79 nC pulse is  $135,800 \pm 600$ .

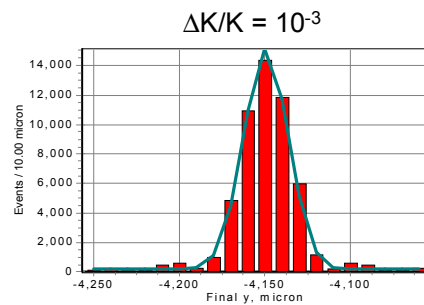
The error on the fit centroid in Figure 9 is dominated by the statistics of the 53192 simulated photons that made it through the grating, diffracted into the positive first order, and interacted in the scintillator to appear in the plot. If the detector were 100% efficient, and the bunch charge were 0.79 nC, the detector would see  $135,800 \pm 600$  photons and the error in the centroid would be less. Fitting only the 53192 simulated photons, as we have done here, is equivalent to having a detector efficiency of 39%.

**Figure 10: Row projection across positive 1st order peak from the first undulator segment with K detuned by  $10^{-3}$  and  $10^{-4}$**



Fitted Centroid:  
 $-4149.34 \pm 0.06 \mu\text{m}$

53,324 simulated photons  
 Scaled to Full Pulse:  $136,000 \pm 600$   
 photons



Fitted Centroid:  
 $-4155.82 \pm 0.06 \mu\text{m}$

53,630 simulated photons  
 Scaled to Full Pulse:  $137,000 \pm 600$   
 photons

Figure 10 shows the row projections for other simulations of the first undulator segment but having a  $K$  value detuned by  $\Delta K/K = 10^{-4}$ , left, and  $\Delta K/K = 10^{-3}$ , right. The shift in the position of the centroid from the nominal value is  $0.64 \pm 0.08 \mu\text{m}$  for the  $\Delta K/K = 10^{-4}$  detuning and  $7.12 \pm 0.08 \mu\text{m}$  for the  $\Delta K/K = 10^{-3}$  detuning, all well enough above the error in the fit centroid to be measurable.

## Grating Performance with the Other Undulator Segments

The Off-Axis Spectrometer Monte Carlo model was run for all nine high resolution single undulator spontaneous datasets. For each run, the MC generated  $10^7$  photons into the solid angle defined by the 2 mm x 2 mm area perpendicular to the beamline axis at 244 meters from the position of the beginning of the first undulator segment and tracked them through the spectrometer simulation. The results are summarized in Table 2.

The solid angle intercepted by the full grating is different for the first, middle, and last undulator segments since they are at different distances from the grating. This will cause a  $z$  dependent shift of the centroid since the shape of the spontaneous is highly sensitive to the integrating aperture. To remedy this the acceptance of the spectrometer was made lower for the middle segment and still lower for the last segment by setting the aperture of the thin Ta slit to the values shown in the 2<sup>nd</sup> and 3<sup>rd</sup> columns of Table 2.

**Table 2: Apertures, Fit Centroids, and Photon Yields, for the single undulator datasets**

DataSet	Horizontal Slit Aperture ( $\mu\text{m}$ )	Vertical Slit Aperture ( $\mu\text{m}$ )	Fit Centroid ( $\mu\text{m}$ )	Monte Carlo #photons	#photons scaled to LCLS Full Pulse
FirstDet-3	2000	200	$-4155.82 \pm 0.06$	53324	$136136 \pm 589$
FirstDet-4	2000	200	$-4149.34 \pm 0.06$	53630	$136917 \pm 591$
FirstNom	2000	200	$-4148.70 \pm 0.06$	53192	$135799 \pm 588$
MidDet-3	1435	143	$-4156.09 \pm 0.08$	30668	$130465 \pm 745$
MidDet-4	1435	143	$-4149.44 \pm 0.08$	30965	$131728 \pm 749$
MidNom	1435	143	$-4148.74 \pm 0.08$	31059	$132128 \pm 750$
LastDet-3	870	87.1	$-4155.99 \pm 0.14$	13326	$145253 \pm 1258$
LastDet-4	870	87.1	$-4149.46 \pm 0.14$	13365	$145678 \pm 1260$
LastNom	870	87.1	$-4148.80 \pm 0.14$	13094	$142725 \pm 1247$

The next two columns in table 2 list the centroid and errors obtained from Gaussian fits to the Monte Carlo simulations for the nine high-resolution datasets. Note that the centroid errors grow larger for undulator segments further downstream. This

error reflects the decrease in simulated photons that reach the detector in the ROI. This decrease in simulated photons is due to the fact that the  $10^7$  starting photons were generated in different solid angles (all were generated to fill the 2 mm x 2 mm area at 244 meters from the position of the beginning of the first undulator segment, thus the distance and solid angle to the other segments is a function of their position) hence represent different fractions of the full pulse. The last column in Table 2 shows the expected number of photons in the ROI scaled to a full 0.79 nC pulse. The scaled values are the same to within errors across all undulator segments indicating that the solid angle intercepted by the spectrometer is the same for all segments.

## K Analysis

In practice we will use one of the segments as a standard and compare the data from the other segments to it. For the purposes of this study we use the dataset *LastNom*, representing the last undulator segment at the nominal  $K$  value, as our standard. We

**Table 3: Spectral Measurements Summary**

Relative Centroid Shift:  $\bar{X}_i$   $i^{\text{th}}$  DataSet Fit Centroid  
 $\frac{\Delta\bar{X}_i}{\bar{X}} = \frac{\bar{X}_i - \bar{X}_{LastNom}}{\bar{X}_{LastNom}}$   $\bar{X}_{LastNom}$  Last Segment, nominal  $K$ , Fit Centroid

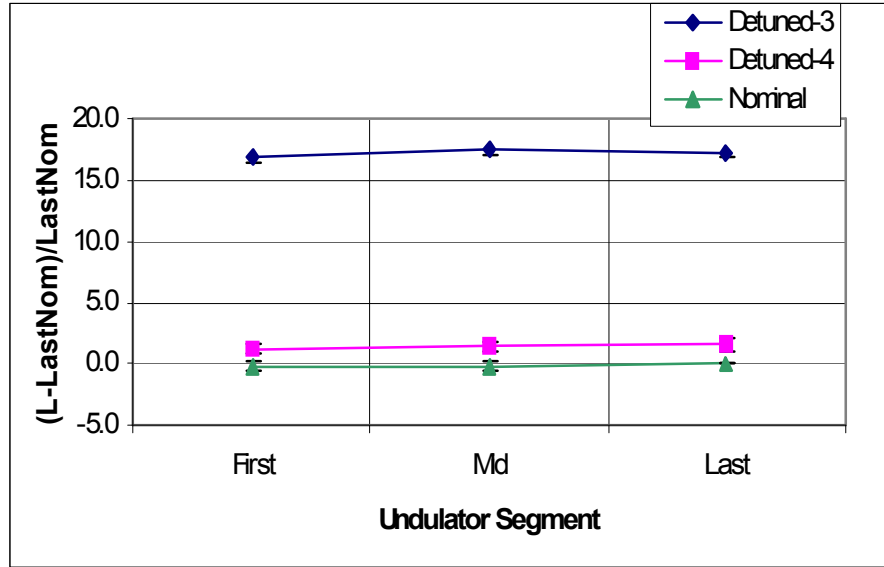
DataSet	Fit Centroid ( $\mu\text{m}$ )	Relative Centroid Shift X 10 <sup>4</sup>
FirstDet-3	-4155.82 $\pm$ 0.06	16.9 $\pm$ 0.4
FirstDet-4	-4149.34 $\pm$ 0.06	1.3 $\pm$ 0.4
FirstNom	-4148.70 $\pm$ 0.06	-0.3 $\pm$ 0.4
MidDet-3	-4156.09 $\pm$ 0.08	17.6 $\pm$ 0.4
MidDet-4	-4149.44 $\pm$ 0.08	1.5 $\pm$ 0.4
MidNom	-4148.74 $\pm$ 0.08	-0.2 $\pm$ 0.4
LastDet-3	-4155.99 $\pm$ 0.14	17.3 $\pm$ 0.5
LastDet-4	-4149.46 $\pm$ 0.14	1.6 $\pm$ 0.5
LastNom	-4148.80 $\pm$ 0.14	0.0

then compare  $\bar{X}_i$ , the fit centroid results of the  $i^{\text{th}}$  data set to  $\bar{X}_{LastNom}$ , the fit centroid result for the *LastNom* data set, by calculating the relative centroid shift:

$$\frac{\Delta\bar{X}_i}{\bar{X}} = \frac{\bar{X}_i - \bar{X}_{LastNom}}{\bar{X}_{LastNom}}$$

of each of the other segments. If all spectra have the same shape, the fit centroids are proportional to the  $K$  values of the segments and the

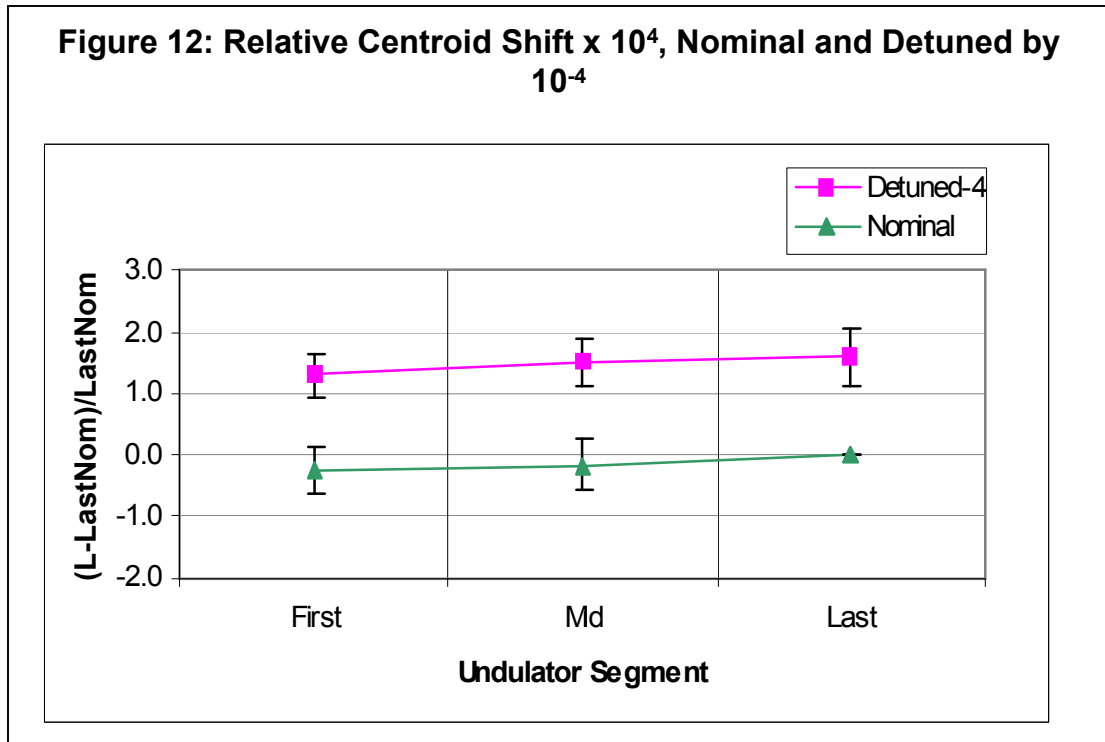
**Figure 11 : Relative Centroid Shift x 10<sup>4</sup>, all data**



relative centroid shifts will be equal to the relative  $K$  errors:  $\frac{\Delta \bar{X}_i}{\bar{X}} = \frac{\Delta K_i}{K}$ . The results are tabulated in Table 3 and plotted in figures 11 and 12 to show any trends in the data.

Firstly, there is a clear difference between the last segment at its nominal  $K$  setting and the other segments when  $K$  is detuned by  $10^{-3}$  (table 3 and Figure 11.) We see relative centroid shifts in this case of  $17.3 \pm 0.5$  for the last segment,  $17.6 \pm 0.4$  for the mid segment, and  $16.9 \pm 0.4$ , all within errors of the expected value of 17.7. Secondly, when  $K$  is detuned by  $10^{-4}$ , the effect is smaller, and in this case we see relative centroid shifts of  $1.6 \pm 0.5$  for the last segment,  $1.5 \pm 0.4$  for the middle segment, and  $1.3 \pm 0.4$  for the first segment, again within errors of the expected value of 1.77 (table 3 and Figure 12.) Finally, the table shows that the first, middle, and last segments at nominal  $K$  have relative centroid shifts that are consistent with zero. This is also illustrated in Figure 12, which plots the data for the nominal and detuned by  $10^{-4}$  datasets.

Looking at all of the points in Figure 12 one observes a possible downward trend in the data suggesting a possible Z dependence in the measured centroids amounting to a perceived change in  $K$  of  $\frac{\Delta K}{K} \approx 0.25 \times 10^{-4}$  over the length of the undulator stack. This trend could be due to the fact that the grating / zoneplate is focused on the middle undulator segment. For this study the effect is smaller than the errors on measuring individual undulator segments and is ignored.

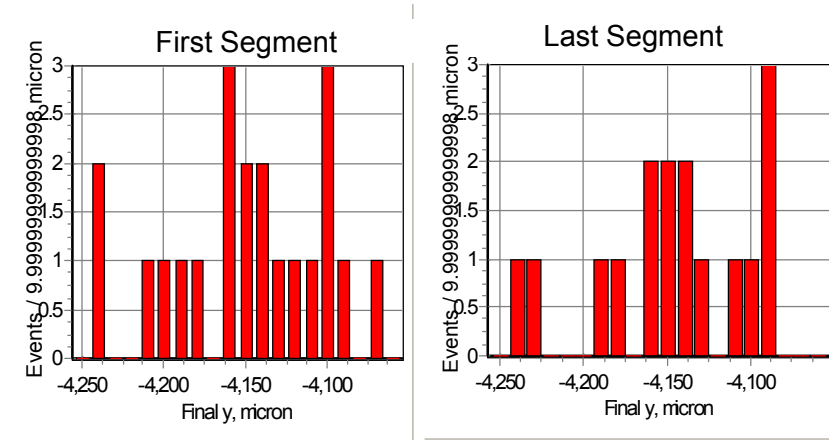


## Background

The above described MC runs simulated only a small portion of the radiation given off by the undulator segments, namely those photons between 8.0 and 8.5 keV emitted into the solid angle defined by the 2 mm x 2 mm area perpendicular to the beamline axis at 244 meters from the position of the beginning of the first undulator segment. To check for possible backgrounds from the other photons that may swamp our signal we performed simulations using a nearly complete distribution of emitted photons namely those photons between 0 and 24 MeV emitted into the solid angle defined by a 120 mm x 40 mm area perpendicular to the beamline axis at 244 meters from the position of the beginning of the first undulator segment. The large solid angle and energy range of this full simulation contains > 90% of the photon emission.

Figure 13 shows the distribution of photons that stopped in the scintillator ROI for the full simulation of the first undulator segment, left, and the last undulator segment, right. In all, 21 (first) and 16 (last) of the  $10^7$  simulated photons stopped in the scintillator in these full simulations. (In the last segment simulation, one simulated photon passed through the ROI but did not stop in the scintillator.) Since these simulations span the full energy range they do contain some number of signal photons (between 8.0 and 8.5 keV) so we do expect some photons in the

**Figure 13: Results of full range background simulations**



21 simulated photons stop  
Scaled to Full Pulse:  $91,000 \pm 21,000$   
photons

16 simulated photons stop  
Scaled to Full Pulse:  $84,000 \pm 21,000$   
photons  
1 simulated photon passes through  
Scaled to Full Pulse:  $5,000 \pm 5,000$   
photons

distributions. The scaling factors for these runs are 4339 and 5274 so when scaled to a full 0.79 nC pulse, the 21 and 16 stopping photons represent  $91000 \pm 21000$  and  $84000 \pm 21000$  photons/pulse respectively and this is very close to the 130,000 to 140,000 photons / pulse of signal photons that we determined from the high resolution runs. Therefore there is no excess above the expected signal indicating that there is no significant background with this configuration.

Nevertheless even though the full simulation contains nearly all photon types, very few photons of higher energy are actually generated because of the limited statistics. The high-energy photons are potentially problematic since they can penetrate the slit material and any that stop in the scintillator can deposit a lot of energy. To study the high-energy photons in greater detail, we simulated  $10^7$  photons from just the portion of the energy spectrum  $> 500$  keV. These runs had scale factors of only 23.4 and 23.3 for the first and last segments. We found that 11 of the  $10^7$  simulated high energy photons arrived at the scintillator for the last segment simulation but none arrived at the scintillator from the first segment. This

is presumably due to the greater distance of the first segment that allows the high energy photons to attain greater transverse distance at the scintillator position. None of the 11 photons from the first segment stopped in the scintillator. When scaled to a full 0.79 nC pulse this implies  $260 \pm 80$  photons passing through the scintillator ROI per pulse and  $< 23$  stopping from the first segment and  $< 23$  photons passing through the scintillator ROI per pulse and  $< 23$  stopping from the last segment. This indicates that there is no significant background from the very high-energy portion of the spontaneous spectrum for this type of thin scintillator detector.

## Conclusion

This study shows how a 200 nm period transmission grating with an transverse area of 200 micron x 2 mm can be used to measure the relative  $K$  values of single undulator segments. The simulations show that the grating will give clear, single shot spectra over the spontaneous fundamental with at least 130,000 photons per pulse in the spectral region of interest with minimal background from higher energy spontaneous radiation. As expected, the fitted centroids of these spectra are strictly proportional to the undulator segment  $K$  value to a precision limited by the statistics of the number of photons detected in the spectrometer Region of Interest. Assuming a detector having 10 micron spatial resolution and an efficiency of 30 to 50%, the simulation shows that a  $10^{-4}$  relative difference in  $K$  between the first, middle, or last undulator segments produces a shift in the spectral centroid of at least 3 standard deviations and should therefore be measurable. Moreover, it is likely that a reflection grating, with potentially larger aperture and smaller effective period could be significantly more sensitive.